

Over-the-Air Majority Vote Computation with Modulation on Conjugate-Reciprocal Zeros

Alphan Şahin, *Member, IEEE*

Abstract—In this study, we propose a new approach to compute the majority vote (MV) function based on modulation on conjugate-reciprocal zeros (MOCZ) and introduce three different methods. In these methods, each transmitter maps the votes to the zeros of a Huffman polynomial, and the corresponding polynomial coefficients are transmitted. The receiver evaluates the polynomial constructed by the elements of the superposed sequence at conjugate-reciprocal zero pairs and detects the MV with a direct zero-testing (DiZeT) decoder. With differential and index-based encoders, we eliminate the need for power-delay information at the receiver while improving the computation error rate (CER) performance. The proposed methods do not use instantaneous channel state information at the transmitters and receiver. Thus, they provide robustness against phase and time synchronization errors. We theoretically analyze the CERs of the proposed methods. Finally, we demonstrate their efficacy in a distributed median computation scenario.

Index Terms—Huffman polynomials, single-carrier waveform, over-the-air computation, zeros of polynomials

I. INTRODUCTION

With more applications relying on data exchange across many distributed nodes over wireless networks, meeting the time requirements under limited communication bandwidth becomes increasingly challenging. One of the prominent approaches to reduce the latency for these scenarios is over-the-air computation (OAC) [2]–[4]. With OAC, a multivariate function is aimed to be computed by relying on its representation that can structurally match with the underlying operation that multiple-access wireless channel naturally performs. The remarkable gain obtained with OAC is that latency does not scale with the number of nodes since multi-user interference is harnessed for computation through simultaneous transmissions [5]. OAC has been considered for a wide range of applications, such as wireless federated learning [6], distributed localization [7], wireless data centers [8], and wireless control systems [9]. However, achieving a reliable computation with OAC is difficult because signal superposition occurs after the channel distorts the signals. In this work, we focus on this fundamental problem and propose an OAC scheme that does not rely on the availability of channel state information (CSI) at the transmitters and receiver, based on a recently proposed method, i.e., *modulation on conjugate-reciprocal zeros (MOCZ)* [10]–[12].

In the literature, there is a substantial effort to overcome fading channels for OAC [5], [13]–[16]. A commonly used

technique is channel inversion at the transmitter, where the transmitter multiplies the parameters with the inverses of the channel coefficients before transmission [17]–[21]. While this solution ensures coherent signal superposition, it is sensitive to phase errors at the transmitters, as the receiver cannot fix the potential phase errors with linear equalizers. Phase synchronization can be very challenging in practice because of the inevitable hardware impairments such as clock errors, residual carrier frequency offset (CFO), calibration errors, and jittery time synchronization. For instance, a large phase rotation in the frequency domain can occur because of sample deviations at the transmitter or receiver [22]. Also, non-stationary channel conditions can deteriorate the coherent signal superposition in mobile environments [23]. To eliminate the need for phase synchronization, non-coherent OAC schemes that exploit the energy of the superposed signals have been studied in the literature. For instance, in type-based multiple access (TBMA), the nodes transmit on orthogonal resources allocated for different classes (i.e., types), and the frequency histogram is estimated to compute statistical averages [24], [25]. In [26] and [7], two orthogonal resources representing the local gradient directions (i.e., 1 and -1 as votes) are allocated, and the norms of received symbols on these resources are compared with each other to compute the majority vote (MV) for the global gradient direction. Similarly, in [27], the digits of the parameters are proposed to be aggregated on orthogonal resources dedicated to all possible numerals in a balanced number system. An alternative non-coherent OAC solution is Goldenbaum’s scheme [28], [29]. In this method, a random unimodular sequence is multiplied by the square root of the parameter to be aggregated. At the receiver, the norm-square of the received sequence is calculated to estimate the aggregated parameter. Although this method can provide robustness against synchronization errors, it can suffer from interference terms due to the loss of orthogonality between the sequences. It is also worth noting that non-coherent OAC schemes demonstrably work in practice without introducing stringent requirements. For instance, in [22], the distributed training based on MV computation is demonstrated with off-the-shelf software-defined radios (SDRs). Goldenbaum’s scheme is also shown in practice in [30].

With OAC, a set of special functions, i.e., nomographic functions, can be computed. Several examples of nomographic functions are arithmetic mean, weighted sum, modulo-2 sum, polynomial function, maximum, product, and MV [5]. In this work, we are interested in computing the MV function with OAC. MV function is utilized for a wide

Alphan Şahin is with the Electrical Engineering Department, University of South Carolina, Columbia, SC, USA. E-mail: asahin@mailbox.sc.edu

This paper was submitted in part to the IEEE Global Communications Conference 2024 [1].

variety of applications. For example, [19], [26], and [31] implement distributed training based on MV [32] over wireless networks with OAC. In [7], the MV function is employed for distributed localization with the motivation of enhanced security. In [33], MV is considered for unmanned aerial vehicle (UAV) waypoint flight control. Another appealing feature of the MV function is that it can be used for median computation, as discussed further in Section V. Compared to the arithmetic mean, aggregating parameters based on the median can provide immunity against outliers or Byzantine attacks [34], [35].

MOCZ is a non-linear modulation technique where information bits are encoded into the zeros of a polynomial, and the transmitted sequence corresponds to the polynomial coefficients [10]. As comprehensively analyzed in [11], the merit of MOCZ is that the zero structure of the transmitted signal is preserved at the receiver regardless of channel impulse response (CIR). This property is because the convolution operation can be represented as a polynomial multiplication, and the zeros are unaffected by the multiplication operation. As a result, MOCZ enables the receiver to obtain the information bits without the knowledge of instantaneous CSI. Although the idea of modulation on zeros can be used with an arbitrary set of polynomials, the zeros of a polynomial can be very sensitive to perturbation of its coefficients (e.g., Wilkinson's polynomial [36]). To achieve robustness against additive noise, in [11], the authors propose to use Huffman polynomials [37], discussed further in Section II. In the literature, MOCZ is evaluated and improved in various scenarios. For instance, in [12], the authors investigate the practical aspects of MOCZ and assess its performance under impairments like carrier frequency and time offsets. In [38], MOCZ is investigated along with discrete Fourier transform-spread orthogonal frequency division multiplexing (DFT-s-OFDM) and extended to multi-user scenarios. In [39], the correlation properties of Huffman sequences are exploited to achieve joint radar and communications with MOCZ at 60 GHz millimeter wave band. In [40], the authors consider multiple antennas and develop a non-coherent Viterbi-like detector to achieve diversity gain. In [41], the authors consider an over-complete system for MOCZ based on faster-than-Nyquist signaling to improve spectral efficiency. To our knowledge, MOCZ has not been studied for OAC in the literature.

In this work, inspired by MOCZ, we strive to answer how the zeros of polynomials can be utilized for OAC. Using the zeros of polynomials for OAC is challenging since the signal superposition changes the original zeros of the polynomials at the transmitters non-linearly. Our main contribution lies in addressing this mathematical challenge and showing that we can encode the zeros of polynomials for OAC without using the CSI at the transmitters or receiver. Our specific contributions can be listed as follows:

- We introduce a new approach to compute the MV function based on MOCZ. The key property that we use is that when a linear combination of polynomials is evaluated at a specific value, and if this particular value corresponds to a zero of a polynomial in the combinations, the contribution of that polynomial to the

evaluation is zero. Based on this property and Lemmas 1-3, we prove that a non-coherent aggregation can be achieved in the fading channel and a direct zero-testing (DiZeT) decoder, initially proposed for communications with MOCZ in [11], can be used to obtain the MVs.

- We propose three methods, each with its own advantages. While Method 1 provides the highest computation rate, it requires delay profile information. We address this issue by using a differential encoding strategy in Method 2 at the expense of halved computation rate. Finally, by extending our preliminary results in [1], we reduce the computation error rate (CER) by introducing redundancy in Method 3 with an index-based encoder. Also, we analytically derive the CERs in Corollaries 3-5 based on Lemma 4. All methods are robust to time and phase synchronization errors as they do not rely on the availability of CSI at the transmitters and receiver.
- We assess each method's performance with comprehensive simulations and demonstrate the applicability of the proposed methods to a distributed median computation scenario using MVs.

Organization: The rest of the paper is organized as follows. Section II provides the system model. In Section III, we discuss the proposed OAC methods in detail. In Section IV, we theoretically analyze the CERs of the proposed methods. In Section V, we provide numerical results and assess the methods in a distributed median computation scenario. We conclude the paper in Section VI.

Notation: The sets of complex and real numbers are denoted by \mathbb{C} and \mathbb{R} , respectively. The function $\text{sign}(\cdot)$ results in 1, -1 , or 0 for a positive, a negative, or a zero-valued argument, respectively. $\mathbb{E}_x[\cdot]$ is the expectation of its argument over all random variables. The zero-mean circularly symmetric complex Gaussian distribution with variance σ^2 is denoted by $\mathcal{CN}(0, \sigma^2)$. The uniform distribution with the support between a and b is $\mathcal{U}_{[a,b]}$. The function $\mathbb{I}[\cdot]$ results in 1 if its argument holds; otherwise, it is 0. The probability of an event A is denoted by $\Pr(A; x)$, where x is a parameter to calculate the probability.

II. SYSTEM MODEL

Consider an OAC scenario with U transmitters and a receiver, where all radios are equipped with a single antenna. Let $t_n^{(u)} \in \mathbb{C}$ be the n th element of sequence $\mathbf{t}^{(u)}$ to be transmitted from the u th transmitter over an orthogonal waveform. Assume that the impact of the composite channel between the u th transmitter and the receiver on the received sequence is convolutive and the corresponding impulse response is $\mathbf{h}^{(u)} = (h_0^{(u)}, \dots, h_{L_e-1}^{(u)})$, where $L_e \geq 1$ is the number of effective taps.¹ All transmitters access the medium concurrently for computation. We can then express the n th

¹The composite channel is a function of the multipath channel and the waveform. For instance, for OFDM, each subcarrier is exposed to a single-tap channel (i.e., $L_e = 1$) regardless of the power-delay profile of the multipath channel if the cyclic prefix duration is large enough. On the other hand, L_e can be larger than 1 for a single-carrier waveform after matched filtering.

received element $r_n \in \mathbb{C}$ at the receiver after the signal superposition as

$$r_n = \left(\sum_{u=1}^U \sum_{l=0}^{L_e-1} \sqrt{P_u} h_l^{(u)} t_{n-l}^{(u)} \right) + \omega_n, \quad (1)$$

where $h_l^{(u)} \sim \mathcal{CN}(0, \rho_l)$ is the channel coefficient on the l th tap for the u th transmitter, P_u is the average transmit power of the u th transmitter, and $\omega_n \sim \mathcal{CN}(0, \sigma_{\text{noise}}^2)$ is the additive white Gaussian noise (AWGN). Without loss of generality, we consider exponential decay to model the composite channel between the u th transmitter and the receiver as

$$\rho_l = \mathbb{E} \left[|h_l^{(u)}|^2 \right] = \begin{cases} \frac{1-\rho}{1-\rho^{L_e}} \rho^l, & \rho < 1 \\ \frac{1}{L_e}, & \rho = 1 \end{cases}, \quad (2)$$

for $\sum_{l=0}^{L_e-1} \rho_l = 1$, where $\rho \in (0, 1]$ is a decay constant [11].

We assume that the *average* received signal powers of the transmitters are aligned with a power control mechanism [42]. Thus, the relative positions of the transmitters to the receiver do not change our analyses as in [18], [19], [43]. Also, we set $P_u, \forall u$, to 1 Watt and calculate the average signal-to-noise ratio (SNR) of a transmitter at the receiver as $\text{SNR} = 1/\sigma_{\text{noise}}^2$.

Let $\mathbf{x}^{(u)} = (x_0^{(u)}, x_1^{(u)}, \dots, x_K^{(u)})$ denote the complex-valued coefficients of the polynomial function $X^{(u)}(z) = x_K^{(u)} z^K + x_{K-1}^{(u)} z^{K-1} + \dots + x_0^{(u)}$ for $z \in \mathbb{C}$ and $x_K^{(u)} \neq 0$. We set $t_n^{(u)}$ as

$$t_n^{(u)} = \begin{cases} x_n^{(u)}, & 0 \leq n \leq K \\ 0, & \text{otherwise} \end{cases}. \quad (3)$$

Since a convolution operation in discrete time can be represented by a polynomial multiplication in the z -domain, we can express the received sequence $\mathbf{r} = (r_0, \dots, r_{K+L_e-1})$ in (1) as

$$R(z) = \underbrace{\sum_{u=1}^U X^{(u)}(z) H^{(u)}(z)}_{\triangleq S(z)} + W(z), \quad (4)$$

where $W(z)$ is the z -domain representation of the noise sequence $\mathbf{w} = (w_0, \dots, w_{K+L_e-1})$, and $X^{(u)}(z)$ and $H^{(u)}(z)$ are the z -domain representations of $\mathbf{x}^{(u)}$ and $\mathbf{h}^{(u)}$, respectively, i.e.,

$$X^{(u)}(z) = \sum_{n=0}^K x_n^{(u)} z^n = x_K^{(u)} \prod_{k=0}^{K-1} (z - \alpha_k^{(u)}), \quad (5)$$

and

$$H^{(u)}(z) = \sum_{l=0}^{L_e-1} h_l^{(u)} z^l = h_{L_e-1}^{(u)} \prod_{l=0}^{L_e-2} (z - \gamma_l^{(u)}), \quad (6)$$

by using the facts that $X^{(u)}(z)$ and $H^{(u)}(z)$ have K and L_e-1 complex-valued roots, respectively, by the fundamental theorem of algebra.

A. Preliminaries on Huffman Sequences

Let $\mathbf{x} \triangleq (x_0, x_1, \dots, x_K)$ denote the complex-valued coefficients of the polynomial function $X(z) = \sum_{n=0}^K x_n z^n = x_K \prod_{k=0}^{K-1} (z - \alpha_k)$, for $x_K \neq 0$. We define the aperiodic auto-correlation function (AACF) of the sequence \mathbf{x} as $A(z) \triangleq z^K \sum_{\ell=-K}^K a_\ell z^\ell$, where a_ℓ is the ℓ th aperiodic auto-correlation coefficient of the sequence \mathbf{x} , given by

$$a_\ell \triangleq \begin{cases} \sum_{n=0}^{K-\ell} x_n^* x_{n+\ell}, & 0 \leq \ell \leq K \\ \sum_{n=0}^{K+\ell} x_n x_{n-\ell}^*, & -K \leq \ell < 0 \\ 0, & \text{otherwise} \end{cases}. \quad (7)$$

A Huffman sequence and a Huffman polynomial can then be defined as follows:

Definition 1 (Huffman sequence and Huffman polynomial). *The sequence \mathbf{x} and the polynomial $X(z)$ are called a Huffman sequence and Huffman polynomial, respectively, if $A(z) = \bar{\eta} + \|\mathbf{x}\|_2^2 z^K + \eta z^{2K}$ for $\eta = x_K \bar{x}_0$.*

Notice that the AACF $A(z)$ can be directly calculated from the zeros of $X(z)$ as [11]

$$\begin{aligned} A(z) &= z^K X(z) \overline{X(1/\bar{z})} \\ &= x_K \bar{x}_0 \prod_{k=0}^{K-1} (z - \alpha_k) \prod_{k=0}^{K-1} (z - \frac{1}{\bar{\alpha}_k}). \end{aligned} \quad (8)$$

In [37], by exploiting the K th root of unity and conjugate-reciprocal zero pairs of $A(z)$ in (8), i.e., $\{(\alpha_k, \frac{1}{\bar{\alpha}_k}), \forall k\}$, Huffman shows that the K zeros of a Huffman polynomial are evenly placed on two reciprocal circles centered at the origin, and their amplitudes can be either d or d^{-1} for $d > 1$, i.e., $\alpha_k \in \mathcal{Z}_k \triangleq \{d e^{\frac{j2\pi k}{K}}, d^{-1} e^{\frac{j2\pi k}{K}}\}$. Thus, for a given d , 2^K distinct Huffman sequences with an identical AACF can be synthesized.

The AACFs of Huffman sequences are very close to impulse function. Hence, they can be useful for radar applications [44]. In [11] and [12], it is shown that the zeros of Huffman polynomials are numerically stable when the corresponding polynomial coefficients are perturbed with additive noise and can be utilized for modulation, leading to binary modulation on conjugate-reciprocal zeros (BMOCZ). At the transmitter, an information bit is encoded into one of the zeros in a conjugate-reciprocal zero pair. At the receiver side, a low-complexity non-coherent detector that compares two metrics by evaluating the polynomial at the zeros of a conjugate-reciprocal zero pair, i.e., DiZeT detector, is employed to detect the information bits without CSI.

Given their numerical stability, we consider Huffman sequences for $\mathbf{x}^{(u)}$ in this work. We normalize $\|\mathbf{x}^{(u)}\|_2^2$ to $K+1$ by setting $x_K^{(u)}$ (see (5)) as

$$x_K^{(u)} = \sqrt{\frac{\eta(K+1)}{\prod_{k=0}^{K-1} |\alpha_k^{(u)}|}}, \quad (9)$$

for $\eta = 1/(d^K + d^{-K})$ and $d \triangleq \sqrt{1 + \sin(\pi/K)}$. Note that this specific value of d maximizes the minimum distance between the zeros to improve the robustness against noise for a DiZeT decoder [11].

B. Problem Statement

Suppose that the fading coefficients, i.e., $\{\mathbf{h}^{(u)}, \forall u\}$, are not available at the transmitters and the receiver, and the receiver is interested in computing M MV functions expressed as

$$m_\ell = \text{sign} \left(\sum_{u=1}^U v_\ell^{(u)} \right), \quad \forall \ell \in \{0, 1, \dots, M-1\}, \quad (10)$$

where $v_\ell^{(u)} \in \{-1, 1\}$ represents the ℓ th vote of u th transmitter and $m_\ell \in \{-1, 1\}$ is the ℓ th MV. *How can the MVs be calculated with OAC by exploiting the zeros of polynomials while still being agnostic to the CSI at the transmitters and receiver?* Although MOCZ allows the receiver to use non-coherent detectors to obtain the bits for single-user communications, it is not trivial to use the same concept for computation in the channel as the signal superposition for $U > 1$ in (4) changes the original zeros of the polynomials at the transmitters non-linearly.

Example 1. Consider the Huffman polynomials given by

$$\begin{aligned} X^{(1)}(z) &= \sqrt{\frac{12}{17}} \left(z - \frac{1}{2} \right) (z + 2) = \sqrt{\frac{12}{17}} \left(z^2 + \frac{3}{2}z - 1 \right), \\ X^{(2)}(z) &= \sqrt{\frac{12}{17}} \left(z - 2 \right) \left(z + \frac{1}{2} \right) = \sqrt{\frac{12}{17}} \left(z^2 - \frac{3}{2}z - 1 \right), \end{aligned}$$

for $\eta = 4/17$, $d = 2$, and $K = 2$. In an ideal channel, the sum of these polynomials can be obtained as

$$S(z) = X^{(1)}(z) + X^{(2)}(z) = 2\sqrt{\frac{12}{17}}(z-1)(z+1),$$

which demonstrates that the zeros of $S(z)$ are non-trivial functions of the zeros of $X^{(1)}(z)$ and $X^{(2)}(z)$.

III. PROPOSED METHODS

In this section, we discuss three methods to compute MVs. We introduce Lemmas 1-3, which allow us to derive the statistics that estimate the number of nodes voting for 1 and -1 and the corresponding detectors. For the derivations, we need the following functions related to channel and noise:

$$\begin{aligned} \Gamma(d) &\triangleq \mathbb{E} \left[|H^{(u)}(de^{\frac{j2\pi\ell}{K}})|^2 \right] = \sum_{l=0}^{L_e-1} \mathbb{E} \left[|h_l^{(u)} d^l e^{\frac{j2\pi\ell l}{K}}|^2 \right] \\ &= \sum_{l=0}^{L_e-1} \rho_l d^{2l} = \begin{cases} \frac{1-\rho}{1-\rho^{L_e}} \frac{1-d^{2L_e} \rho^{L_e}}{1-d^2 \rho}, & \rho < 1 \\ \frac{1}{L_e} \frac{1-d^{2L_e}}{1-d^2}, & \rho = 1 \end{cases}. \quad (11) \end{aligned}$$

and

$$\Omega(d) \triangleq \mathbb{E} \left[\left| W(de^{\frac{j2\pi\ell}{K}}) \right|^2 \right] = \sigma_{\text{noise}}^2 \frac{1-d^{2(K+L_e)}}{1-d^2}. \quad (12)$$

It is worth noting that an arbitrary delay profile can also be considered for $\Gamma(d)$ without changing the derivations in the following subsections.

A. Method 1: Uncoded MV Computation

In this method, we compute $M = K$ MVs without any coding and the u th transmitter sets the k th root of $X^{(u)}(z)$ based on the vote $v_\ell^{(u)}$, $\forall \ell \in \{0, 1, \dots, K-1\}$, as

$$\alpha_k^{(u)} = \begin{cases} \frac{1}{d} e^{\frac{j2\pi k}{K}}, & v_k^{(u)} = 1 \\ d e^{\frac{j2\pi k}{K}}, & v_k^{(u)} = -1 \end{cases}. \quad (13)$$

The encoding in (13) is very similar to BMOCZ in [11]. However, since the transmitted signals superpose for OAC in (4), it is not trivial how to design the detector to detect the MVs. We use the following lemma to develop the decoder:

Lemma 1. Let U_ℓ^+ and U_ℓ^- denote the number of transmitters with positive and negative votes for the ℓ th MV computation. For the mapping in (13) with $\Pr(v_\ell^{(u)} = 1) = \Pr(v_{\ell'}^{(u)} = -1) = 1/2$, $\forall \ell', \ell' \neq \ell$,

$$\mathbb{E} \left[\left| S(de^{\frac{j2\pi\ell}{K}}) \right|^2 \right] = U_\ell^+ \mathcal{X}_1(d) \Gamma(d), \quad (14)$$

where

$$\begin{aligned} \mathcal{X}_1(d) &\triangleq \eta(K+1)(d-d^{-1})^2 d^K \\ &\times \frac{1}{2^{K-1}} \prod_{k=1}^{K-1} \left(|1 - e^{\frac{j2\pi k}{K}}|^2 + |d - d^{-1} e^{\frac{j2\pi k}{K}}|^2 \right), \quad (15) \end{aligned}$$

where the expectation in (14) is over the distributions of channels and votes.

The proof is given in Appendix A.

Corollary 1. $\mathbb{E} \left[\left| S(d^{-1} e^{\frac{j2\pi\ell}{K}}) \right|^2 \right]$ can be calculated by replacing with U_ℓ^+ and d with U_ℓ^- and d^{-1} in (14), respectively.

The key observation from Lemma 1 and Corollary 1 is that the expected values of $|S(de^{\frac{j2\pi\ell}{K}})|^2$ and $|S(d^{-1} e^{\frac{j2\pi\ell}{K}})|^2$ are linearly scaled by U_ℓ^+ and U_ℓ^- , respectively. Thus, a DiZeT decoder, initially used for detecting bits [11], can still be utilized to compute the ℓ th MV with proper scalars highlighted by Lemma 1 and Corollary 1 as

$$\hat{m}_\ell = \text{sign}(\tilde{U}_\ell^+ - \tilde{U}_\ell^-), \quad (16)$$

where \tilde{U}_ℓ^+ and \tilde{U}_ℓ^- are the unbiased estimates of U_ℓ^+ and U_ℓ^- , respectively, given by

$$\tilde{U}_\ell^+ = \frac{\left| R(de^{\frac{j2\pi\ell}{K}}) \right|^2 - \Omega(d)}{\mathcal{X}_1(d) \Gamma(d)}, \quad (17)$$

and

$$\tilde{U}_\ell^- = \frac{\left| R(d^{-1} e^{\frac{j2\pi\ell}{K}}) \right|^2 - \Omega(d^{-1})}{\mathcal{X}_1(d^{-1}) \Gamma(d^{-1})}. \quad (18)$$

Note that (16) can be simplified by using $\mathcal{X}_1(d)/\mathcal{X}_1(d^{-1}) = d^{2K}$, but it still requires the delay profile of the channel.

Example 2. For $d = 2$ and $K = 2$, $\mathcal{X}_1(d)$ and $\mathcal{X}_1(d^{-1})$ are approximately 32.5588 and 2.0349, respectively, and their ratio is 16.

The computation rate for Method 1 can also be obtained as K MVs over $K + L_e$ complex-valued resources. The number of consumed resources is $K + L_e$ as the transmitted sequence needs to be padded with L_e zeros to express (4).

B. Method 2: Differential MV Computation

In this method, we use differential encoding to compute $M = K/2$ MVs and the u th transmitter sets the k th and $(k + 1)$ th roots of $X^{(u)}(z)$ based on the vote $v_\ell^{(u)}$, $\forall \ell \in \{0, 1, \dots, K/2 - 1\}$, as

$$(\alpha_{2k'}^{(u)}, \alpha_{2k'+1}^{(u)}) = \begin{cases} \left(\frac{1}{d} e^{\frac{j2\pi 2k'}{K}}, de^{\frac{j2\pi(2k'+1)}{K}} \right), & v_{k'}^{(u)} = 1 \\ \left(de^{\frac{j2\pi 2k'}{K}}, \frac{1}{d} e^{\frac{j2\pi(2k'+1)}{K}} \right), & v_{k'}^{(u)} = -1 \end{cases} \quad (19)$$

for $k' = \lfloor k/2 \rfloor$. To derive the corresponding detector, we use the following lemma:

Lemma 2. Let U_ℓ^+ and U_ℓ^- denote the number of transmitters with positive and negative votes for ℓ th MV computation. For the mapping in (19) with $\Pr(v_{\ell'}^{(u)} = 1) = \Pr(v_{\ell'}^{(u)} = -1) = 1/2$, $\forall \ell', \ell' \neq \ell$,

$$\mathbb{E} \left[\left| S \left(de^{\frac{j2\pi 2\ell}{K}} \right) \right|^2 \right] = U_\ell^+ \mathcal{X}_2(d) \Gamma(d), \quad (20)$$

where

$$\begin{aligned} \mathcal{X}_2(d) &\triangleq \eta(K+1)(d-d^{-1})^2 |1 - e^{\frac{2\pi}{K}}|^2 d^K \\ &\times \frac{1}{2^{\frac{K}{2}-1}} \prod_{k=1}^{\frac{K}{2}-1} |1 - e^{\frac{j2\pi 2k}{K}}|^2 |d - d^{-1} e^{\frac{j2\pi(2k+1)}{K}}|^2 \\ &+ |1 - e^{\frac{j2\pi(2k+1)}{K}}|^2 |d - d^{-1} e^{\frac{j2\pi 2k}{K}}|^2, \end{aligned} \quad (21)$$

where the expectation in (20) is over the distributions of channels and votes.

The proof is given in Appendix B.

Corollary 2. $\mathbb{E} \left[\left| S \left(de^{\frac{j2\pi(2\ell+1)}{K}} \right) \right|^2 \right]$ can be calculated by replacing U_ℓ^+ with U_ℓ^- in (20).

With Lemma 2 and Corollary 2, the unbiased estimates of U_ℓ^+ and U_ℓ^- can be obtained as

$$\tilde{U}_\ell^+ = \frac{\left| R \left(de^{\frac{j2\pi 2\ell}{K}} \right) \right|^2 - \Omega(d)}{\mathcal{X}_2(d) \Gamma(d)}, \quad (22)$$

and

$$\tilde{U}_\ell^- = \frac{\left| R \left(de^{\frac{j2\pi(2\ell+1)}{K}} \right) \right|^2 - \Omega(d)}{\mathcal{X}_2(d) \Gamma(d)}, \quad (23)$$

respectively. Hence, the ℓ th MV can be computed as

$$\hat{m}_\ell = \text{sign} \left(\left| R \left(de^{\frac{j2\pi(2\ell+1)}{K}} \right) \right|^2 - \left| R \left(de^{\frac{j2\pi 2\ell}{K}} \right) \right|^2 \right). \quad (24)$$

Compared with the detector in Method 1, the detector in (24) does not need the delay profile of the channel to compute the MVs. The price paid for this benefit is a reduced computation rate, i.e., $K/2$ MVs over $K + L_e$ complex-valued resources.

C. Method 3: Index-based MV Computation

In this approach, we compute $M = \log_2(K)$ MVs, and the roots of $X^{(u)}(z)$ are modulated based on an index calculated by using all votes. To this end, let $b_\ell^{(u)} \in \mathbb{Z}_2$ be a binary representation of the vote $v_\ell^{(u)}$ as $b_\ell^{(u)} \triangleq (v_\ell^{(u)} + 1)/2$ for $\forall \ell \in \{0, 1, \dots, \log_2(K) - 1\}$. The u th transmitter sets the k th root of $X^{(u)}(z)$ as

$$\alpha_k^{(u)} = \begin{cases} \frac{1}{d} e^{\frac{j2\pi k}{K}}, & \sum_{\ell=0}^{M-1} b_\ell^{(u)} 2^\ell = k \\ de^{\frac{j2\pi k}{K}}, & \text{otherwise} \end{cases}. \quad (25)$$

For instance, we obtain $\sum_{\ell=0}^{M-1} b_\ell^{(u)} 2^\ell = 0$ for $v_\ell^{(u)} = -1$, $\forall \ell$, as $b_\ell^{(u)} = 0$, $\forall \ell$. Hence, the radius of the 0th root is d^{-1} , while the radius of any other root for $k \neq 0$ is set to d .

Lemma 3. Let U_ℓ^+ and U_ℓ^- denote the number of transmitters with positive and negative votes for ℓ th MV computation. For the mapping in (25) with $\Pr(v_{\ell'}^{(u)} = 1) = \Pr(v_{\ell'}^{(u)} = -1) = 1/2$, $\forall \ell'$ and $\ell' \neq \ell$,

$$\mathbb{E} \left[\left| S \left(de^{\frac{j2\pi \ell}{K}} \right) \right|^2 \right] = \frac{U_\ell^+ \mathbb{I}[l_\ell = 1] + U_\ell^- \mathbb{I}[l_\ell = 0]}{2^{\log_2(K)-1}} \mathcal{X}_3(d) \Gamma(d), \quad (26)$$

with

$$\mathcal{X}_3(d) \triangleq \eta(K+1)(d-d^{-1})^2 d^K K^2, \quad (27)$$

where the expectation in (26) is over the distribution of channels and votes and $l = \sum_{i=0}^{M-1} l_i 2^i$ with $l_i \in \mathbb{Z}_2$, $\forall i$.

The proof is given in Appendix C.

Based on Lemma 3, we can obtain unbiased estimates of U_ℓ^+ and U_ℓ^- as

$$\tilde{U}_\ell^+ = \frac{\sum_{l=0, l_\ell=1}^{K-1} \left| R \left(de^{\frac{j2\pi l}{K}} \right) \right|^2 - \frac{K}{2} \Omega(d)}{\mathcal{X}_2(d) \Gamma(d) 2^{-\log_2(K)+1}}, \quad (28)$$

and

$$\tilde{U}_\ell^- = \frac{\sum_{l=0, l_\ell=0}^{K-1} \left| R \left(de^{\frac{j2\pi l}{K}} \right) \right|^2 - \frac{K}{2} \Omega(d)}{\mathcal{X}_2(d) \Gamma(d) 2^{-\log_2(K)+1}}, \quad (29)$$

respectively, and derive the detector to obtain the ℓ th MV as

$$\hat{m}_\ell = \text{sign} \left(\sum_{l_\ell=1}^{K-1} \left| R \left(de^{\frac{j2\pi l}{K}} \right) \right|^2 - \sum_{l_\ell=0}^{K-1} \left| R \left(de^{\frac{j2\pi l}{K}} \right) \right|^2 \right). \quad (30)$$

Compared with Method 1 and Method 2, Method 3 uses $K/2$ measurements for each test in (30) to determine the MVs. Hence, as demonstrated in Section V, it yields a better CER at the expense of a lower computation rate, i.e., $\log_2(K)$ MVs over $K + L_e$ complex-valued resources. Also, the detector does not need the delay profile information. Note that Method 3 reduces to Method 2 for $K = 2$.

In Fig. 1, we exemplify the zero placements for Methods 1-3 and $K = 8$. In Fig. 1(a), we assume that the votes at the transmitter are $(v_0^{(u)}, \dots, v_7^{(u)}) = (-1, -1, 1, 1, -1, -1, 1, 1)$. By following (13), the zeros (see the points marked by stars in Fig. 1(a)) are chosen based on the values of

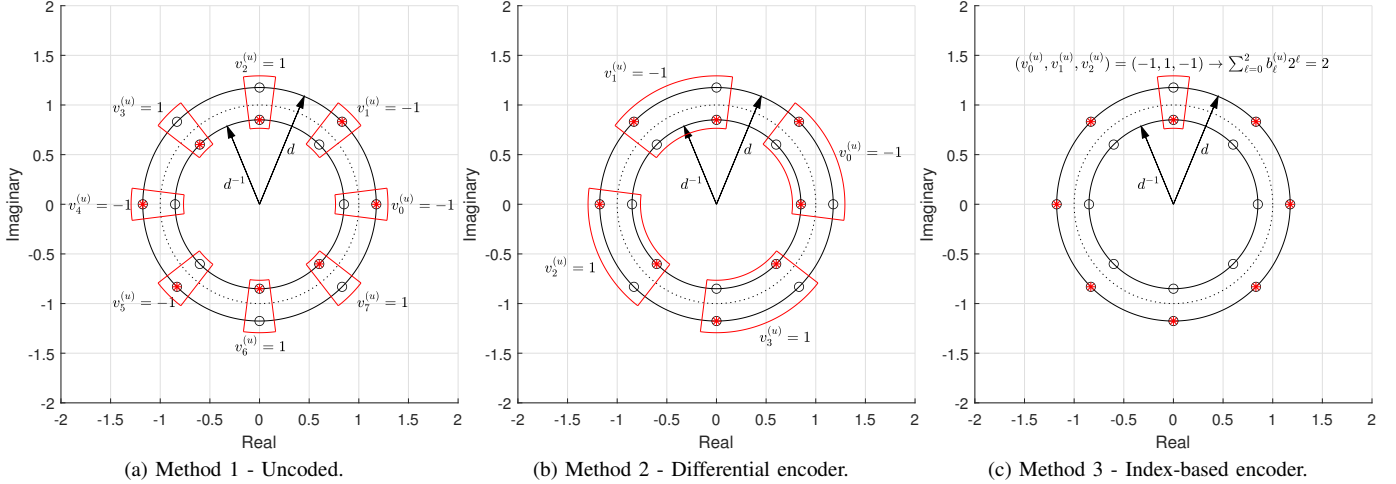


Fig. 1. Example zero placements for Methods 1-3. The star and circle markers indicate the chosen zeros and the possible zero locations for a Huffman polynomial, respectively.

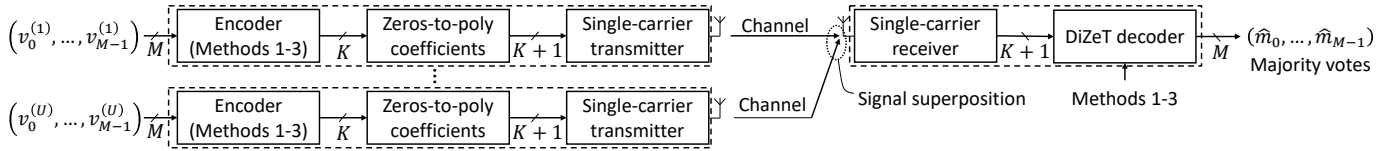


Fig. 2. Transmitter and receiver block diagrams.

TABLE I
COMPARISON OF METHODS.

	Method 1	Method 2	Method 3
CSI	Not required	Not required	Not required
PDP	Required	Not required	Not required
Rate	$\frac{K}{K+L_e}$	$\frac{K/2}{K+L_e}$	$\frac{\log_2(K)}{K+L_e}$
Reliability	Low	Low	High

$v_\ell^{(u)}$. In Fig. 1(b), we consider Method 2, and the votes are $(v_0^{(u)}, v_1^{(u)}, v_2^{(u)}, v_3^{(u)}) = (-1, -1, 1, 1)$. In this method, two zeros are allocated for each vote, and the zeros alternate their radii based on the value of the vote by (19). Finally, in Fig. 1(c), we show the zero placement for Method 3 for $(v_0^{(u)}, v_1^{(u)}, v_2^{(u)}) = (-1, 1, -1)$. Since we obtain $\sum_{\ell=0}^{M-1} b_\ell^{(u)} 2^\ell = 2$ for $(b_0^{(u)}, b_1^{(u)}, b_2^{(u)}) = (0, 1, 0)$ from (25), the zero indexed by $k = 2$ changes its position while the other zeros remain on the circle with the radius d . In TABLE I, we summarize the pros and cons of the proposed methods.

Finally, we provide the transmitter and receiver block diagrams in Fig. 2. After the encoder generates the zeros, i.e., a zero codeword of length K , the zero codeword is converted to polynomial coefficients of length $K + 1$. After the conversion, the polynomial coefficients are transmitted with a single-carrier transmitter (e.g., upsampling and pulse shaping). We refer the reader to [45] for the variants of a single-carrier waveform. The receiver receives the sum of the transmitted signals. After processing the superposed signal with a single-carrier receiver (e.g., matched filter and down-sampling), the receiver uses a DiZeT decoder, i.e., (16), (24),

or (30), to obtain the MVs. It is worth noting that the proposed methods can also be utilized with orthogonal frequency division multiplexing (OFDM) as long as the elements of the encoded sequence are mapped to multiple OFDM symbols and subcarriers *within* the coherence time and bandwidth (i.e., $L_e = 1$ tap).

D. Complexity Analysis and Numerical Stability

On the transmitter side, converting the encoded zeros to polynomial coefficients introduces an additional complexity to the radio. In [11, Eq. (8)], it is shown that the conversion can be handled with an iterative algorithm that incrementally builds the polynomial function by using each zero one step at a time. The time complexity of this algorithm is $\mathcal{O}(K^2)$. As noted in [11], MATLAB's `poly` function also uses the same expansion algorithm.² It is also possible to reduce the complexity to $\mathcal{O}(K \log^2(K))$ by recursively grouping the zeros into halves and using the fast Fourier transform for polynomial multiplication.

Based on our analysis, the `poly` function does not provide numerically stable results for large K values. To address this issue, we use the implementation based on the derivation in Appendix D. In this method, we evaluate the polynomial function at $z = e^{j2\pi \frac{p}{K+1}}$ for $p \in \{0, 1, \dots, K\}$ by using its zeros, and calculate the $(K + 1)$ -point inverse discrete Fourier transform (IDFT) of the resulting sequence to obtain the polynomial coefficients. This algorithm evaluates (51) for $K + 1$ different values, each requiring K multiplications.

²The version of MATLAB is 2024a.

Thus, the time complexity of this method is also $\mathcal{O}(K^2)$. However, it is more stable than the poly function as it does not accumulate the numerical errors through iterations.

On the receiver side, the complexity increases because of evaluating the polynomial $R(z)$ at $2K$ zeros with DiZeT decoders, i.e., (16), (24), and (30). The complexity of evaluating an n th order polynomial function is $\mathcal{O}(n)$ with Horner's method [46]. Thus, the additional time complexity due to a DiZeT decoder can be obtained as $\mathcal{O}(K^2)$. Note that the numerical stability of Horner's method can be improved further with state-of-the-art solutions (e.g., see [47] and the references therein).

IV. COMPUTATION-ERROR RATE ANALYSIS

For Methods 1-3, we can express the CER for the ℓ th MV as

$$\text{CER}_\ell = \begin{cases} \Pr(\tilde{U}_\ell^+ - \tilde{U}_\ell^- < 0), & U_\ell^+ > U_\ell^- \\ 1 - \Pr(\tilde{U}_\ell^+ - \tilde{U}_\ell^- < 0), & U_\ell^+ < U_\ell^- \\ 1, & U_\ell^+ = U_\ell^- \end{cases}, \quad (31)$$

where the third case in (31) is because $\text{sign}(\tilde{U}_\ell^+ - \tilde{U}_\ell^-)$ is almost surely not zero due to the noisy reception in communication channels. We can also express $\Pr(\tilde{U}_\ell^+ - \tilde{U}_\ell^- < 0)$ as

$$\begin{aligned} \Pr(\tilde{U}_\ell^+ - \tilde{U}_\ell^- < 0) &= \mathbb{E}_{\mathbf{V}} \left[F_{\tilde{U}_\ell^+ - \tilde{U}_\ell^-}(x; \mathbf{V}) \right] \\ &= \frac{1}{2^{M(U-1)}} \sum_{\forall \mathbf{V}} F_{\tilde{U}_\ell^+ - \tilde{U}_\ell^-}(x; \mathbf{V}), \end{aligned} \quad (32)$$

where $F_{\tilde{U}_\ell^+ - \tilde{U}_\ell^-}(x; \mathbf{V})$ is the cumulative distribution function (CDF) of $\tilde{U}_\ell^+ - \tilde{U}_\ell^-$ given all votes $\mathbf{V} \triangleq (\mathbf{u}_\ell, \dot{\mathbf{V}})$ for $\mathbf{u}_\ell = (\mathbf{1}_{U_\ell^+}, -\mathbf{1}_{U_\ell^-})$ and $\dot{\mathbf{V}} \triangleq (\mathbf{u}_1, \dots, \mathbf{u}_{\ell-1}, \mathbf{u}_{\ell+1}, \dots, \mathbf{u}_U)$. Hence, we need an analytical expression of $F_{\tilde{U}_\ell^+ - \tilde{U}_\ell^-}(0; \mathbf{V})$ to obtain $\Pr(\tilde{U}_\ell^+ - \tilde{U}_\ell^- < 0)$. To this end, we use the following result from [33]:

Lemma 4 ([33]). *Let a_l and b_l be independent exponential random variables with the rate λ_{a_l} and λ_{b_l} , respectively, $\forall l \in \{0, \dots, K-1\}$. For $A = \sum_{l=0}^{K-1} a_l$ and $B = \sum_{l=0}^{K-1} b_l$, $F_{A-B}(x)$ can be calculated as*

$$F_{A-B}(x) = \frac{1}{2} - \int_{-\infty}^{\infty} \frac{\varphi_a(t)\varphi_b^*(t)}{2\pi jt} e^{-jtx} dt, \quad (33)$$

where

$$\varphi_a(t) = \prod_{l=0}^{K-1} \frac{1}{1 - jt\lambda_{a_l}^{-1}}, \quad (34)$$

and

$$\varphi_b(t) = \prod_{l=0}^{K-1} \frac{1}{1 - jt\lambda_{b_l}^{-1}}. \quad (35)$$

Lemma (4) exploits the characteristic functions of the exponential distribution, convolution theorem, and the inversion formula given in [48]. We can now calculate the $F_{\tilde{U}_\ell^+ - \tilde{U}_\ell^-}(0; \mathbf{V})$ for Methods 1-3 theoretically as follows:

Corollary 3. $F_{\tilde{U}_\ell^+ - \tilde{U}_\ell^-}(0; \mathbf{V})$ for Method 1 can be calculated by evaluating (33) at $x = \Omega(d)/(\mathcal{X}_1(d)\Gamma(d)) - \Omega(d^{-1})/(\mathcal{X}_1(d^{-1})\Gamma(d^{-1}))$ for

$$\varphi_a(t) = \frac{1}{1 - jt\lambda_+^{-1}}, \quad (36)$$

and

$$\varphi_b(t) = \frac{1}{1 - jt\lambda_-^{-1}}, \quad (37)$$

with

$$\lambda_+^{-1} = \frac{1}{\mathcal{X}_1(d)} \sum_{u=1}^U |X^{(u)}(de^{\frac{j2\pi l}{K}})|^2 + \frac{\Omega(d)}{\mathcal{X}_1(d)\Gamma(d)},$$

and

$$\lambda_-^{-1} = \frac{1}{\mathcal{X}_1(d^{-1})} \sum_{u=1}^U |X^{(u)}(d^{-1}e^{\frac{j2\pi l}{K}})|^2 + \frac{\Omega(d^{-1})}{\mathcal{X}_1(d^{-1})\Gamma(d^{-1})}.$$

Corollary 4. $F_{\tilde{U}_\ell^+ - \tilde{U}_\ell^-}(0; \mathbf{V})$ for Method 3 can be calculated by evaluating (33) at $x = 0$ with

$$\varphi_a(t) = \prod_{\substack{l=0 \\ \ell=1}}^{K-1} \frac{1}{1 - jt\lambda_l^{-1}}, \quad (38)$$

and

$$\varphi_b(t) = \prod_{\substack{l=0 \\ \ell=0}}^{K-1} \frac{1}{1 - jt\lambda_l^{-1}}, \quad (39)$$

for $\lambda_l^{-1} = \Gamma(d) \sum_{u=1}^U |X^{(u)}(de^{\frac{j2\pi l}{K}})|^2 + \Omega(d)$.

The proofs of Corollary 3 and Corollary 4 are deferred to Appendix E.

Corollary 5. *Since Method 3 reduces to Method 2 for $K = 2$, the CER for Method 2 can be also directly calculated by using Corollary (4).*

It is worth emphasizing that the integral in (33) can be evaluated numerically for a given set of rate values for Methods 1-3. Also, the sum in (32) can be intractable for large U and M . To address this issue, we calculate the average of the integral in (33) over a few realizations of \mathbf{V} , as done in [33] in this study.

V. NUMERICAL RESULTS

In this section, we assess the proposed methods numerically. We first generate the results on CER, peak-to-mean envelope power ratio (PMEPR), and resource utilization per MV computation. We then apply the proposed methods to a specific application, i.e., distributed median computation. We also compare our results with Goldenbaum's non-coherent OAC scheme in [28] and the coherent OAC scheme in [19], i.e., one-bit broadband digital aggregation (OBDA). For Goldenbaum's method, we map the votes -1 and 1 to the symbols 0 and 2 , respectively. Afterward, the square root of the symbol is multiplied with a unimodular random sequence of length L_{seq} . We choose the phase of an element

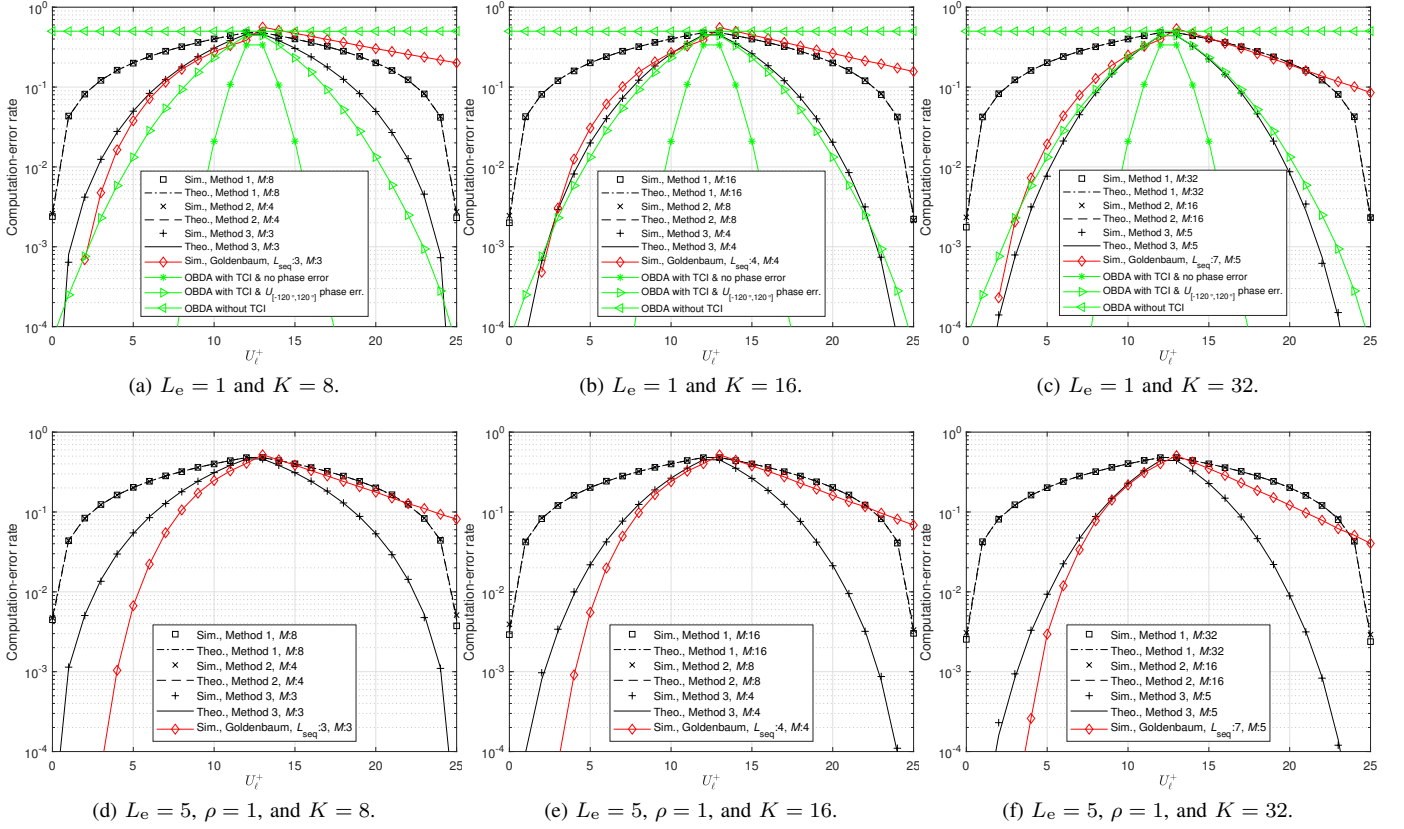


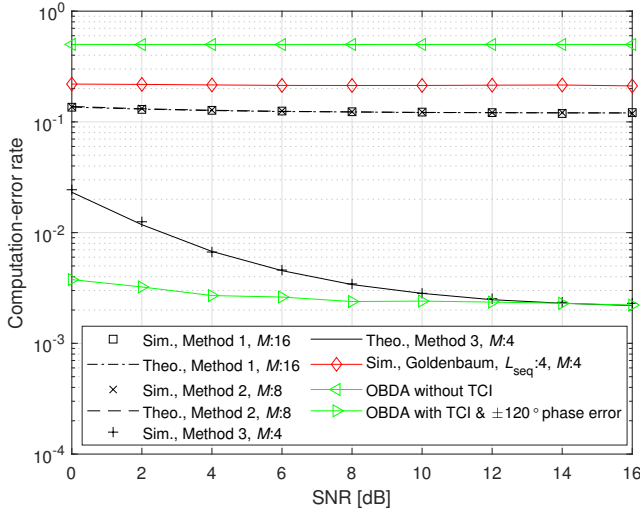
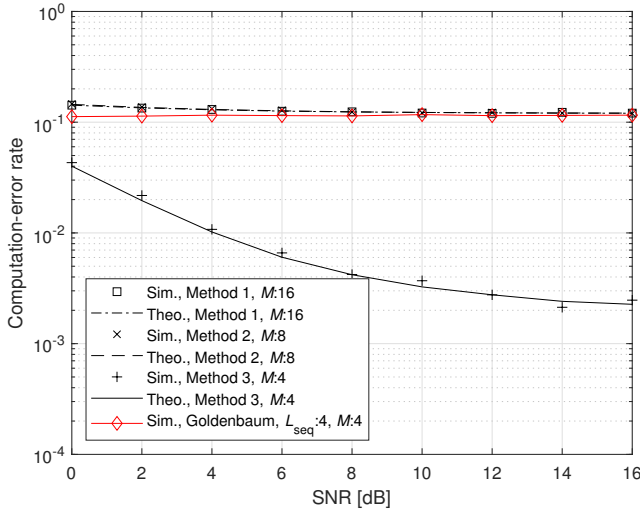
Fig. 3. CER for a given U_ℓ^+ ($U = 25$, SNR = 10 dB).

of unimodular sequence uniformly between 0 and 2π . At the receiver, the norm-square of the aggregated sequences is calculated, and the calculated value is scaled with $f(x) = (x - \sigma_{\text{noise}}^2)/L_{\text{seq}} - U$. Finally, the sign of the scaled value is calculated to obtain the MV. To make a fair comparison, we set L_{seq} to the nearest integer of $(K + 1)/\log_2(K)$, resulting in $M = \log_2(K)$ MVs over $K + 1$ resources as in Method 3, approximately. For instance, for $K = 32$, Method 3 computes 5 MVs by using 33 resources for Method 3. Hence, L_{seq} is set to 7 as $(K + 1)/\log_2(K) \approx 6.6$, and 5 MVs are computed over 35 resources. For OBDA, we map the votes to binary phase shift keying (BPSK) symbols and consider OFDM transmission (i.e., $L_e = 1$). Unless otherwise stated, we use truncated-channel inversion (TCI) for OBDA, where the truncation level is set to 0.2 (i.e., the nodes do not transmit if $|h_0^{(u)}|^2 \leq 0.2$). For comparisons, we also demonstrate the performance of OBDA under phase synchronization errors, where we model the phase error at each node with a uniform probability density function, i.e., $\mathcal{U}_{[-120^\circ, 120^\circ]}$. Note that the superposition is still largely constructive under this model as we use BPSK symbols for OBDA.

In Fig. 3, we demonstrate the CER performance of the schemes for a given number U_ℓ^+ for $U = 25$ transmitters, SNR = 10 dB, and $K \in \{8, 16, 32\}$. In Fig. 3(a)-(c), we consider the case with $L_e = 1$ tap. As can be seen from the results, increasing $|U_\ell^+ - U_\ell^-|$ leads to a better CER for all methods. This result is expected because the distance between two test values for the proposed methods with a

DiZeT decoder increases with $|U_\ell^+ - U_\ell^-|$. The performance of Method 1 and Method 2 are identical in Fig. 3(a)-(c) as we use the scalars in (17) and (18) for Method 1. However, Method 2 does not need a scalar, as seen in (24). Compared to Methods 1-2, Method 3 exploits redundancy and results in a remarkably better CER, and the CER improves further for increasing K at the expense of a reduced computation rate. For Goldenbaum's scheme, the transmitters do not transmit when the devices vote for -1 , and the impact of the channel on the signal decreases for a smaller U_ℓ^+ . Thus, Goldenbaum's scheme causes an asymmetric behavior in CER in the range of U_ℓ^+ , and the CER degrades considerably by increasing for a large U_ℓ^+ . For OBDA, the CER performance is excellent when the nodes have perfect CSI. However, under the phase synchronization errors, the CER increases quickly. Furthermore, if the TCI is not applied at the nodes due to the absence of CSI, OBDA cannot calculate the MV. In Fig. 3(d)-(f), we assess the CER for a frequency-selective channel with $L_e = 5$ taps and $\rho = 1$. Compared to the results in Fig. 3(a)-(c), the CER slightly increases in the selective channel for all proposed methods, while it decreases for Goldenbaum's scheme. Nonetheless, it is still notable that a low-complexity DiZeT-based detector allows the receiver to compute the MVs without knowing the instantaneous CSI at the transmitters and receiver (i.e., without phase and time synchronization across the devices). Finally, the theoretical CER results based on Corollaries 3-5 are well-aligned with the simulation results in Fig. 3.

In Fig. 4, we analyze how the SNR changes the CER for the

(a) $L_e = 1$.(b) $L_e = 5$.Fig. 4. CER for a given SNR ($U = 25$, $U_\ell^+ = 22$, $K = 16$).

same scenario in Fig. 3. For this analysis, we assume $U_\ell^+ = 22$ (i.e., the MV is 1) and $K = 16$, and sweep the SNR from 0 to 16 dB. For all schemes, the CER curves explicitly reveal that increasing SNR does not improve the CER indefinitely. This implies that the distortion due to the fading channel is the main limiting factor for OAC, particularly for non-coherent schemes. Since Method 3 is more reliable than Methods 1-2, increasing SNR leads to a better CER performance. OBDA is more robust than the proposed methods but requires TCI and phase synchronization across the network.

In Fig. 5, we analyze the PMEPR distribution of the transmitted signals for $K \in \{8, 32\}$. For this analysis, we consider DFT-s-OFDM, i.e., a variant of single-carrier waveform maintaining the linear convolution operation in (1) with zero-padding [38], [45], for our methods and Goldenbaum's scheme and OFDM for OBDA. We set the discrete Fourier transform (DFT) and IDFT sizes to $K + 1$ and $16 \times (K + 1)$, respectively, to over-sample the signal in the time domain by a factor of 16. The results in Fig. 5 show that the instantaneous power of the transmitted signals can be high

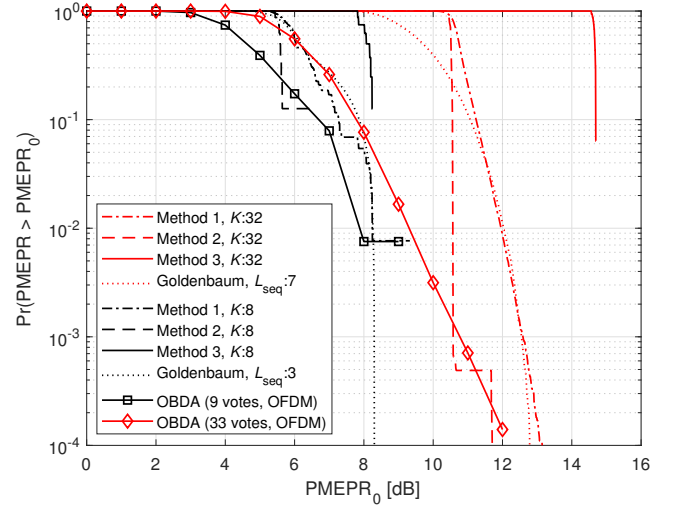


Fig. 5. PMEPR distribution.

and Method 3 causes a higher PMEPR than Methods 1-2. The PMEPR distribution for Goldenbaum's scheme is also similar to Method 2. It is worth noting that the PMEPR distribution of a single-carrier waveform depends on the distribution of the transmitted symbols. For the proposed methods, the elements of sequences originate from Huffman sequences. The magnitude of one of the sequence elements can be higher than that of the other elements in the sequence, leading to a high instantaneous signal power. For OBDA, the PMEPR distribution is a function of the channel selectivity due to the TCI. In Fig. 5, we assume a flat-fading channel for OBDA. While the likelihood of observing an OFDM symbol with a high PMEPR increases with the number of subcarriers for OBDA, its PMEPR characteristics is better than the proposed methods and Goldenbaum's scheme with single-carrier waveform. It is worth noting that the proposed methods can also be used with OFDM, as discussed in Section III. For example, if the coherence bandwidth is sufficiently large, the encoded sequences can be mapped to contiguous OFDM subcarriers. Under this mapping, the PMEPR of the transmitted signals reduce to 1.54 dB and 1.79 dB for $K = 32$, and $K = 8$, respectively, for all methods (not shown in Fig. 5). This appealing result is expected as Huffman sequences have an identical AACF and their impulse-like AACF result in a low PMEPR for OFDM transmission [49]–[51].

In Fig. 6, we compare Methods 1-3 with the case where the receiver computes the MV after it acquires each vote over orthogonal resources (i.e., separation of computation and communication) in terms of resource utilization. For the separation, we assume the spectral efficiency is $\rho = 1$ bps/Hz. Since a vote can be represented with a single bit, we can compute the number of resources needed per MV computation as U/ρ resources. Based on the computation rates discussed in Section III, the number of resources per MV are $(K + L_e)/K$, $(K + L_e)/(K/2)$, and $(K + L_e)/(\log_2(K))$ for Methods 1-3, respectively. In Fig. 6, we plot the number of resources consumed per MV computation for a given number of transmitters U for $K = 32$ zeros and $L_e = 5$ taps. For

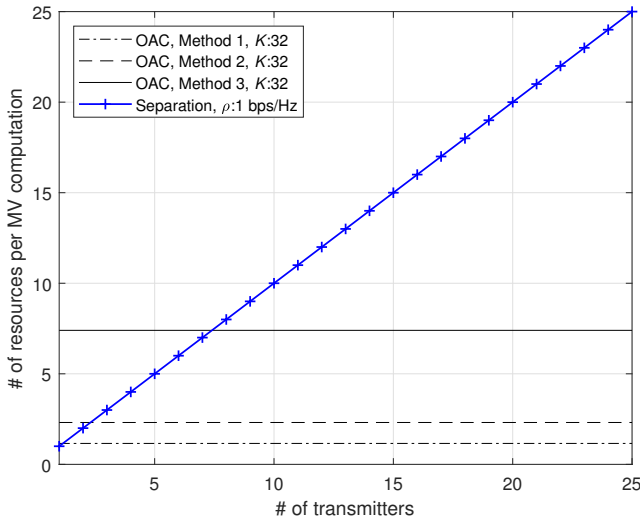


Fig. 6. The number resources consumed per MV computation for a given number of transmitters ($L_e = 1$).

Methods 1-3, the number of resources needed per MV can be calculated as 1.2, 2.3, and 7.4 resources/MV, while it linearly increases with the number of transmitters for the separation. Method 3 becomes more efficient than the separation when at least $U = 8$ devices are in the network.

Next, we evaluate the schemes for a distributed median computation scenario. For this application, let $s_{\ell,u}$ denote the ℓ th parameter at the u th device, and the goal is to compute the median value of the elements in $\{s_{\ell,1}, \dots, s_{\ell,U}\}$ in a distributed manner, $\forall \ell \in \{0, 1, \dots, M-1\}$. To this end, let us express the median as a point minimizing the sum of distances to the parameters at the devices as

$$c_\ell \triangleq \arg \min_c L_\ell(c), \quad (40)$$

where c_ℓ is the median value and $L_\ell(c) = \sum_{u=1}^U \|c - s_{\ell,u}\|_2$ is the corresponding loss function. Since $L_\ell(c)$ is convex, (40) can be solved iteratively as

$$\begin{aligned} \hat{c}_\ell^{(i+1)} &= \hat{c}_\ell^{(i)} - \mu^{(i)} \left. \frac{dL_\ell(c)}{dc} \right|_{c=\hat{c}_\ell^{(i)}} \\ &= \hat{c}_\ell^{(i)} - \mu^{(i)} \sum_{u=1}^U \text{sign}(\hat{c}_\ell^{(i)} - s_{\ell,u}), \end{aligned} \quad (41)$$

where $\hat{c}_\ell^{(i)}$ is an estimate of c_ℓ and $\mu^{(i)}$ is the learning rate at the i th iteration. Since the gradient direction can also be used for solving (40) with an accuracy of $\pm \mu^{(i)}$, (41) can be modified as

$$\hat{c}_\ell^{(i+1)} = \hat{c}_\ell^{(i)} - \mu^{(i)} \text{sign} \left(\sum_{u=1}^U \text{sign}(\hat{c}_\ell^{(i)} - s_{\ell,u}) \right), \quad (42)$$

where the update in (42) is well-aligned with the MV computation problem in (10). In the case of a distributed scenario, the devices do not share their parameters in the network to promote privacy. Instead, the u th device sets the ℓ th vote as $v_\ell^{(u)} = \text{sign}(\hat{c}_\ell^{(i)} - s_{\ell,u})$ for the ℓ th parameter at the i th iteration, and all devices access the spectrum concurrently

for OAC. After the receiver computes the ℓ th MV with OAC and updates $\hat{c}_\ell^{(i)}$ as in (42), it shares $\hat{c}_\ell^{(i+1)}$ in the downlink for the next iteration.

In Fig. 7, we plot the root-mean-squared error (RMSE) of $\hat{c}_\ell^{(i)}$, i.e., the square root of the arithmetic mean of $|\hat{c}_\ell^{(i)} - c_\ell|^2$, over the communication rounds for $K \in \{8, 32, 128\}$ over 1000 realizations. We consider $U = 25$ devices and assume that $s_{\ell,u} \sim \mathcal{U}_{[-\sqrt{3}, \sqrt{3}]}$, $\forall u$, and reduce $\mu^{(i)}$ from 0.01 to $1e-5$ linearly over the iterations. We also generate results when the MV computation occurs without impairments to provide a reference curve. In Fig. 7(a)-(c) and Fig. 7(d)-(f), we consider the scenarios with $L_e = 1$ and $L_e = 5$ taps, respectively. Similar to the CER results in Fig. 3, Method 3 is superior to Methods 1 and 2, while the performance of Method 1 and Method 2 are almost identical. Increasing the number of roots K also improves the performance of Method 3. For instance, the RMSE reduces to 0.002 for $K = 128$ from 0.01 for $K = 8$. Also, the impact of L_e on the RMSE results is negligibly small for the proposed methods. Goldenbaum's scheme performs worse than Method 3 for $L_{\text{seq}} = 3$. However, its performance improves in more selective channels. A larger sequence length L_{seq} leads to a better result, as seen Fig. 3(c). This is because Goldenbaum's method is inherently sensitive to the cross-correlation of the sequences used at the transmitters, and the interference due to the cross-products decreases on average for larger sequence lengths. As expected, OBDA is superior to the proposed methods and Goldenbaum's approach in an ideal scenario, i.e., when the perfect CSI is available. However, under phase synchronization errors, its performance degrades and is similar to that of Method 3. Also, we observe that OBDA does not work without TCI. We observe a large gap between the ideal MV computation scenario and all methods based on OAC. Nonetheless, the OAC does not reveal the votes explicitly to the receiver due to the signal superposition while utilizing the spectrum efficiently through simultaneous transmissions on the same resources. In addition, the proposed OAC methods do not use the CSI at the receiver or transmitters, i.e., reducing the potential overheads.

VI. CONCLUDING REMARKS

In this work, we introduce a new strategy to compute the MV function over the air and discuss three different methods. Fundamentally, the proposed methods rely on nullifying a transmitter's contribution to the superposed value by encoding the votes, i.e., $+1$ and -1 , into the zeros of a Huffman polynomial. We prove that this strategy non-coherently superposes the votes on two different test values, and a DiZeT decoder can be used for MV computation. The proposed methods inherently result in a trade-off between the computation rate, CER, and applicability. Method 1 has the highest computation rate. However, the decoder needs the PDP of the channel a priori. Method 2 improves Method 1's applicability to practice as the decoder does not require the PDP information by using a differential encoder. Method 3 is superior to Method 2 in terms of CER, but the computation rate is reduced further. We analyze the CER theoretically for

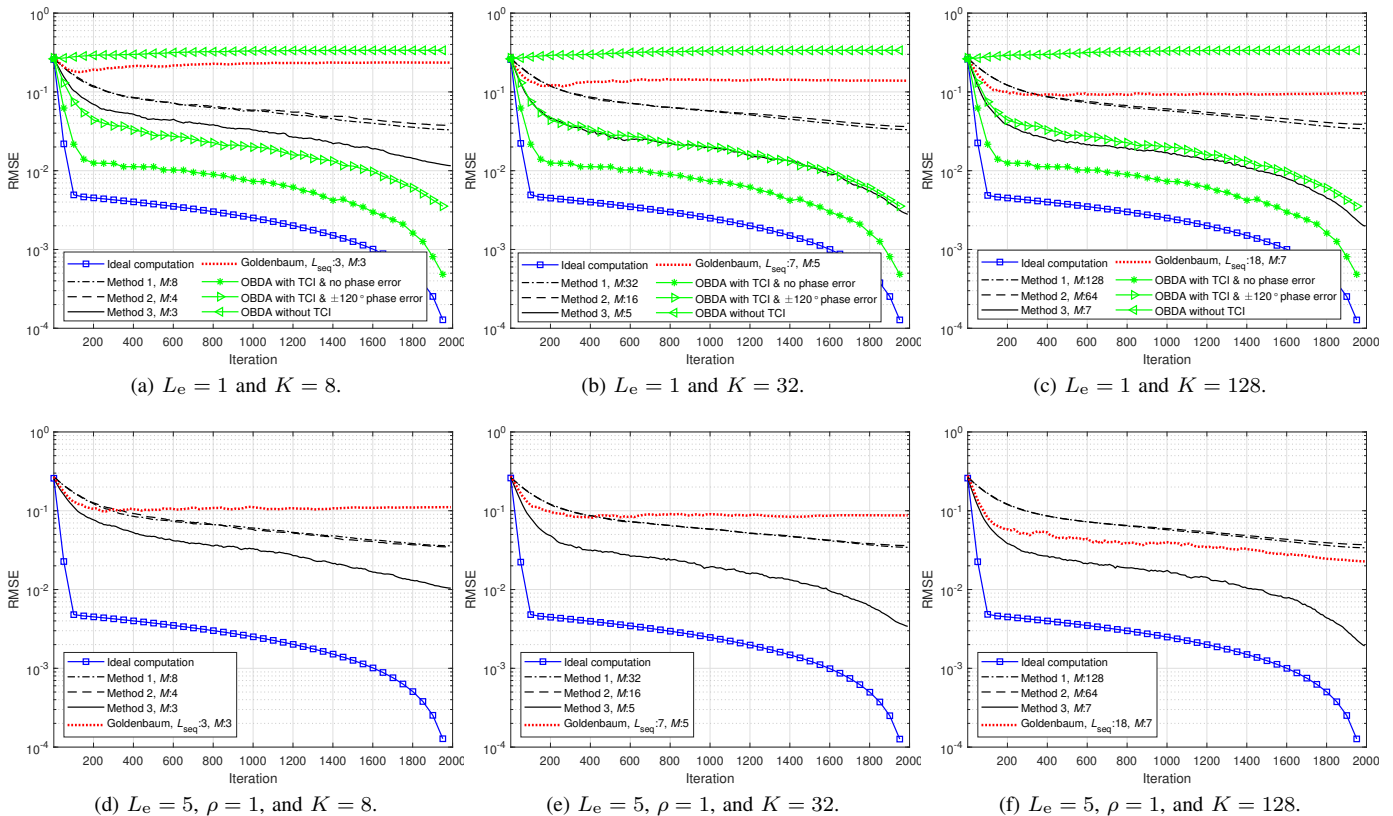


Fig. 7. RMSE for different number of roots and channel length ($U = 25$ transmitters, SNR = 10 dB).

all methods and provide analytical expressions that match the simulation results well. Finally, we show that the proposed methods can be applied to a distributed median computation scenario based on MV computation.

The proposed methods potentially lead to several interesting research directions. For instance, in this work, we choose the radii of roots to maximize the minimum distance between zeros as in [11], [12], [38]. Also, we use two different radii for the roots based on Huffman polynomials. Hence, an unanswered challenge in this work is optimizing the number of radii and their radii for OAC. Secondly, in this work, we consider MV computation. How can we improve the methods for other nomographic functions? In this direction, the representation of integers in binary or balanced systems, as in [27], may be explored. As we demonstrated, the PMEPR of the Huffman sequences for a single-carrier waveform can be high. Hence, another direction is reducing the PMEPR of the transmitted signals for the single-carrier waveform. Finally, assessing the performance of the proposed methods for training a neural network with federated learning is another angle that can be pursued.

APPENDIX A PROOF OF LEMMA 1

Proof of Lemma 1. We can express the right-hand side of (14) as

$$\begin{aligned}
 & \mathbb{E} \left[\left| S \left(de^{\frac{j2\pi\ell}{K}} \right) \right|^2 \right] \\
 & \stackrel{(a)}{=} \sum_{u=1}^U \mathbb{E} \left[\left| H^{(u)} \left(de^{\frac{j2\pi\ell}{K}} \right) \right|^2 \right] \mathbb{E} \left[\left| X^{(u)} \left(de^{\frac{j2\pi\ell}{K}} \right) \right|^2 \right] \\
 & \stackrel{(b)}{=} \sum_{\substack{u=1 \\ v_\ell^{(u)}=1}}^U \mathbb{E} \left[\left| H^{(u)} \left(de^{\frac{j2\pi\ell}{K}} \right) \right|^2 \right] \mathbb{E} \left[\left| X^{(u)} \left(de^{\frac{j2\pi\ell}{K}} \right) \right|^2 \right], \quad (43)
 \end{aligned}$$

where (a) is because the channels and transmitted signals are independent random variables and (b) is because $X^{(u)} \left(de^{\frac{j2\pi\ell}{K}} \right) = 0$ for any u with $v_\ell^{(u)} = -1$. By using (9),

$$\begin{aligned}
 \mathbb{E} \left[\left| X^{(u)} \left(de^{\frac{j2\pi\ell}{K}} \right) \right|^2 \right] &= \mathbb{E} \left[\left| x_K^{(u)} \prod_{k=0}^{K-1} \left(de^{\frac{j2\pi\ell}{K}} - \alpha_k^{(u)} \right) \right|^2 \right] \\
 &= \eta(K+1) \mathbb{E} \left[\prod_{k=0}^{K-1} \frac{\left| de^{\frac{j2\pi\ell}{K}} - \alpha_k^{(u)} \right|^2}{\left| \alpha_k^{(u)} \right|^2} \right]. \quad (44)
 \end{aligned}$$

For any u with $v_\ell^{(u)} = 1$, we can calculate

$$\begin{aligned}
& \mathbb{E} \left[|X^{(u)}(de^{\frac{j2\pi\ell}{K}})|^2 | v_\ell^{(u)} = 1 \right] \\
&= \eta(K+1) \frac{(d-d^{-1})^2}{d^{-1}} \prod_{\substack{k=0 \\ k \neq \ell}}^{K-1} \mathbb{E} \left[\frac{|de^{\frac{j2\pi k}{K}} - \alpha_k^{(u)}|^2}{|\alpha_k^{(u)}|} \right] \\
&= \eta(K+1) \frac{(d-d^{-1})^2}{d^{-1}} \\
&\quad \times \prod_{k=1}^{K-1} \frac{|d - de^{\frac{j2\pi k}{K}}|^2}{d} \frac{1}{2} + \frac{|d - d^{-1}e^{\frac{j2\pi k}{K}}|^2}{d^{-1}} \frac{1}{2} \\
&= \eta(K+1)(d-d^{-1})^2 d^K \\
&\quad \times \frac{1}{2^{\frac{K-1}{2}}} \prod_{k=1}^{K-1} |1 - e^{\frac{j2\pi k}{K}}|^2 + |d - d^{-1}e^{\frac{j2\pi k}{K}}|^2. \quad (45)
\end{aligned}$$

By plugging (11) and (45) in (43), we obtain (14). \square

APPENDIX B PROOF OF LEMMA 2

Proof of Lemma 2. By using the same arguments for (43), we can express the right-hand side of (20) as

$$\begin{aligned}
& \mathbb{E} \left[\left| S(de^{\frac{j2\pi 2\ell}{K}}) \right|^2 \right] \\
&= \sum_{\substack{u=1 \\ v_\ell^{(u)}=1}}^U \mathbb{E} \left[|H^{(u)}(de^{\frac{j2\pi 2\ell}{K}})|^2 \right] \mathbb{E} \left[|X^{(u)}(de^{\frac{j2\pi 2\ell}{K}})|^2 \right]. \quad (46)
\end{aligned}$$

By using (44), for any u with $v_\ell^{(u)} = 1$, we can calculate

$$\begin{aligned}
& \mathbb{E} \left[|X^{(u)}(de^{\frac{j2\pi 2\ell}{K}})|^2 | v_\ell^{(u)} = 1 \right] \\
&= \eta(K+1) \frac{(d-d^{-1})^2}{d^{-1}} \frac{|d - de^{\frac{2\pi}{K}}|^2}{d} \\
&\quad \times \prod_{\substack{k=0 \\ k \neq \ell}}^{\frac{K}{2}-1} \mathbb{E} \left[\frac{|de^{\frac{j2\pi k}{K}} - \alpha_{2k}^{(u)}|^2}{|\alpha_{2k}^{(u)}|} \frac{|de^{\frac{j2\pi k}{K}} - \alpha_{2k+1}^{(u)}|^2}{|\alpha_{2k+1}^{(u)}|} \right] \\
&= \eta(K+1) \frac{(d-d^{-1})^2}{d^{-1}} \frac{|d - de^{\frac{2\pi}{K}}|^2}{d} \\
&\quad \times \prod_{k=1}^{\frac{K}{2}-1} \frac{|d - de^{\frac{j2\pi 2k}{K}}|^2}{d} \frac{|d - d^{-1}e^{\frac{j2\pi(2k+1)}{K}}|^2}{d^{-1}} \frac{1}{2} \\
&\quad + \frac{|d - d^{-1}e^{\frac{j2\pi 2k}{K}}|^2}{d} \frac{|d - de^{\frac{j2\pi(2k+1)}{K}}|^2}{d^{-1}} \frac{1}{2} \\
&= \eta(K+1)(d-d^{-1})^2 |1 - e^{\frac{2\pi}{K}}|^2 d^K \\
&\quad \times \frac{1}{2^{\frac{K}{2}-1}} \prod_{k=1}^{\frac{K}{2}-1} |1 - e^{\frac{j2\pi 2k}{K}}|^2 |d - d^{-1}e^{\frac{j2\pi(2k+1)}{K}}|^2 \\
&\quad + |1 - e^{\frac{j2\pi(2k+1)}{K}}|^2 |d - d^{-1}e^{\frac{j2\pi 2k}{K}}|^2. \quad (47)
\end{aligned}$$

By plugging (11) and (47) in (46), we obtain (20). \square

APPENDIX C PROOF OF LEMMA 3

Proof of Lemma 3. We can express the right-hand side of (26) as

$$\begin{aligned}
& \mathbb{E} \left[\left| S(de^{\frac{j2\pi l}{K}}) \right|^2 \right] \\
&= \sum_{\substack{u=1 \\ \sum_{\ell=0}^{M-1} b_\ell^{(u)} 2^\ell = l}}^U \mathbb{E} \left[|H^{(u)}(de^{\frac{j2\pi l}{K}})|^2 \right] \mathbb{E} \left[|X^{(u)}(de^{\frac{j2\pi l}{K}})|^2 \right] \\
&= \frac{U^+ \mathbb{I}[l \ell = 1] + U_\ell^- \mathbb{I}[l \ell = 0]}{2^{\log_2(K)-1}} \mathbb{E} \left[|H^{(u)}(de^{\frac{j2\pi l}{K}})|^2 \right] \\
&\quad \times \mathbb{E} \left[|X^{(u)}(de^{\frac{j2\pi l}{K}})|^2 \sum_{\ell=0}^{M-1} b_\ell^{(u)} 2^\ell = l \right]. \quad (48)
\end{aligned}$$

By using (44), we can calculate

$$\begin{aligned}
& \mathbb{E} \left[|X^{(u)}(de^{\frac{j2\pi l}{K}})|^2 \sum_{\ell=0}^{M-1} b_\ell^{(u)} 2^\ell = l \right] \\
&= \eta(K+1) \frac{|de^{\frac{j2\pi l}{K}} - d^{-1}e^{\frac{j2\pi l}{K}}|^2}{d^{-1}e^{\frac{j2\pi l}{K}}} \prod_{\substack{k=0 \\ k \neq \ell}}^{K-1} \frac{|de^{\frac{j2\pi k}{K}} - de^{\frac{j2\pi k}{K}}|^2}{|de^{\frac{j2\pi k}{K}}|} \\
&= \eta(K+1)(d-d^{-1})^2 d^K \prod_{k=1}^{K-1} |1 - e^{\frac{j2\pi k}{K}}|^2 \\
&= \eta(K+1)(d-d^{-1})^2 d^K K^2. \quad (49)
\end{aligned}$$

By plugging (11) and (49) in (48), we obtain (26). \square

APPENDIX D FROM ZEROS TO POLYNOMIAL COEFFICIENTS

Consider the polynomial given in (5). Let us define $y_p^{(u)}$ as

$$y_p^{(u)} \triangleq X^{(u)}(z) \Big|_{z=e^{j2\pi \frac{p}{K+1}}}.$$
 (50)

for $p \in \{0, 1, \dots, K\}$. Thus,

$$y_p^{(u)} = \sum_{n=0}^K x_n^{(u)} e^{j2\pi \frac{pn}{K+1}} = x_K^{(u)} \prod_{k=0}^{K-1} (e^{j2\pi \frac{p}{K+1}} - \alpha_k^{(u)}).$$
 (51)

The left-hand side of (51) corresponds to a $(K+1)$ -point IDFT of the sequence $\mathbf{x}^{(u)} = (x_0^{(u)}, x_1^{(u)}, \dots, x_K^{(u)})$. Hence, to obtain $\mathbf{x}^{(u)}$ from the zeros, we apply the $(K+1)$ -point DFT to the right-hand side of (51) as

$$\begin{aligned}
x_n^{(u)} &= \frac{1}{K+1} \sum_{p=0}^K y_p^{(u)} e^{-j2\pi \frac{pn}{K+1}} \\
&= \frac{x_K^{(u)}}{K+1} \sum_{p=0}^K e^{-j2\pi \frac{pn}{K+1}} \prod_{k=0}^{K-1} (e^{j2\pi \frac{p}{K+1}} - \alpha_k^{(u)}) \quad (52)
\end{aligned}$$

for $n \in \{0, 1, \dots, K\}$.

APPENDIX E

PROOFS OF COROLLARY (3) AND COROLLARY (4)

Proof of Corollary (3). By using (17) and (18), we obtain

$$\begin{aligned} & \Pr(\tilde{U}_\ell^+ - \tilde{U}_\ell^- < 0; \mathbf{V}) \\ &= \Pr\left(\frac{\left|R\left(de^{\frac{j2\pi\ell}{K}}\right)\right|^2}{\mathcal{X}_1(d)\Gamma(d)} - \frac{\left|R\left(d^{-1}e^{\frac{j2\pi\ell}{K}}\right)\right|^2}{\mathcal{X}_1(d^{-1})\Gamma(d^{-1})} < x; \mathbf{V}\right) \end{aligned}$$

for $x = \Omega(d)/(\mathcal{X}_1(d)\Gamma(d)) - \Omega(d^{-1})/(\mathcal{X}_1(d^{-1})\Gamma(d^{-1}))$. For a given a set of votes, $|R(de^{\frac{j2\pi\ell}{K}})|^2/(\mathcal{X}_1(d)\Gamma(d))$ is an exponential random variable with the mean λ_+^{-1} because $H^{(u)}(de^{\frac{j2\pi\ell}{K}})$, $\forall u$, and $W(de^{\frac{j2\pi\ell}{K}})$ are independent random variables following zero-mean symmetric complex Gaussian distribution. A similar deduction can be made for $|R(d^{-1}e^{\frac{j2\pi\ell}{K}})|^2/(\mathcal{X}_1(d^{-1})\Gamma(d^{-1}))$, leading to λ_-^{-1} . \square

Proof of Corollary (4). For a given a set of votes, $|R(de^{\frac{j2\pi\ell}{K}})|^2$ is an exponential random variable where its mean is $\lambda_+^{-1} = \Gamma(d) \sum_{u=1}^U |X^{(u)}(de^{\frac{j2\pi\ell}{K}})|^2 + \Omega(d)$ because $H^{(u)}(de^{\frac{j2\pi\ell}{K}})$, $\forall u$, and $W(de^{\frac{j2\pi\ell}{K}})$ are independent random variables following zero-mean symmetric complex Gaussian distribution. \square

REFERENCES

- [1] A. Şahin, "Majority vote computation with modulation on conjugate-reciprocal zeros," in *Proc. IEEE Global Communications Conference (GLOBECOM)*, Dec. 2024, pp. 1–6 (under review).
- [2] B. Nazer and M. Gastpar, "Computation over multiple-access channels," *IEEE Trans. Inf. Theory*, vol. 53, no. 10, pp. 3498–3516, Oct. 2007.
- [3] M. Goldenbaum, H. Boche, and S. Stańczak, "Harnessing interference for analog function computation in wireless sensor networks," *IEEE Trans. Signal Process.*, vol. 61, no. 20, pp. 4893–4906, 2013.
- [4] —, "Nomographic functions: Efficient computation in clustered Gaussian sensor networks," *IEEE Trans. Wireless Commun.*, vol. 14, no. 4, pp. 2093–2105, 2015.
- [5] A. Şahin and R. Yang, "A survey on over-the-air computation," *IEEE Commun. Surveys Tuts.*, vol. 25, no. 3, pp. 1877–1908, Apr. 2023.
- [6] G. Zhu, J. Xu, K. Huang, and S. Cui, "Over-the-air computing for wireless data aggregation in massive IoT," *IEEE Wireless Communications*, vol. 28, no. 4, pp. 57–65, 2021.
- [7] S. S. M. Hoque and A. Şahin, "Chirp-based majority vote computation for federated edge learning and distributed localization," *IEEE Open Journal of the Communications Society*, vol. 4, pp. 1060–1074, 2023.
- [8] X. Wu, S. Zhang, and A. Özgür, "STAC: Simultaneous transmitting and air computing in wireless data center networks," *IEEE Journal on Selected Areas in Communications*, vol. 34, no. 12, pp. 4024–4034, 2016.
- [9] S. Cai and V. K. N. Lau, "Modulation-free M2M communications for mission-critical applications," *IEEE Transactions on Signal and Information Processing over Networks*, vol. 4, no. 2, pp. 248–263, 2018.
- [10] P. Walk, P. Jung, and B. Hassibi, "Short-message communication and FIR system identification using Huffman sequences," in *Proc. IEEE International Symposium on Information Theory (ISIT)*, 2017, pp. 968–972.
- [11] —, "MOCZ for blind short-packet communication: Basic principles," *IEEE Trans. Wireless Commun.*, vol. 18, no. 11, pp. 5080–5097, 2019.
- [12] P. Walk, P. Jung, B. Hassibi, and H. Jafarkhani, "MOCZ for blind short-packet communication: Practical aspects," *IEEE Trans. Wireless Commun.*, vol. 19, no. 10, pp. 6675–6692, 2020.
- [13] U. Altun, G. Karabulut Kurt, and E. Ozdemir, "The magic of superposition: A survey on simultaneous transmission based wireless systems," *IEEE Access*, vol. 10, pp. 79 760–79 794, 2022.
- [14] Z. Chen, E. G. Larsson, C. Fischione, M. Johansson, and Y. Malitsky, "Over-the-air computation for distributed systems: Something old and something new," *IEEE Network*, pp. 1–7, 2023.
- [15] H. Hellström, J. M. B. da Silva Jr., M. M. Amiri, M. Chen, V. Fodor, H. V. Poor, and C. Fischione, "Wireless for machine learning: A survey," *Foundations and Trends in Signal Processing*, vol. 15, no. 4, pp. 290–399, 2022.
- [16] Z. Wang, Y. Zhao, Y. Zhou, Y. Shi, C. Jiang, and K. B. Letaief, "Over-the-air computation for 6G: Foundations, technologies, and applications," *IEEE Internet of Things Journal*, pp. 1–25, 2024.
- [17] M. M. Amiri and D. Gündüz, "Federated learning over wireless fading channels," *IEEE Trans. Wireless Commun.*, vol. 19, no. 5, pp. 3546–3557, Feb. 2020.
- [18] G. Zhu, Y. Wang, and K. Huang, "Broadband analog aggregation for low-latency federated edge learning," *IEEE Trans. Wireless Commun.*, vol. 19, no. 1, pp. 491–506, Jan. 2020.
- [19] G. Zhu, Y. Du, D. Gündüz, and K. Huang, "One-bit over-the-air aggregation for communication-efficient federated edge learning: Design and convergence analysis," *IEEE Trans. Wireless Commun.*, vol. 20, no. 3, pp. 2120–2135, Nov. 2021.
- [20] W. Guo, R. Li, C. Huang, X. Qin, K. Shen, and W. Zhang, "Joint device selection and power control for wireless federated learning," *IEEE J. Sel. Areas Commun.*, vol. 40, no. 8, pp. 2395–2410, 2022.
- [21] J. Yao, Z. Yang, W. Xu, D. Niyato, and X. You, "Imperfect CSI: A key factor of uncertainty to over-the-air federated learning," *IEEE Wireless Communications Letters*, vol. 12, no. 12, pp. 2273–2277, 2023.
- [22] A. Şahin, "A demonstration of over-the-air-computation for FEEL," in *Proc. IEEE Global Communications Conference Workshops (GLOBECOM WRKSHWP) - Edge Learning over 5G Mobile Networks and Beyond*, Dec. 2022, pp. 1–7.
- [23] H. Jung and S.-W. Ko, "Performance analysis of UAV-enabled over-the-air computation under imperfect channel estimation," *IEEE Wireless Commun. Lett.*, pp. 1–1, Nov. 2021.
- [24] G. Mergen and L. Tong, "Type based estimation over multiaccess channels," *IEEE Trans. Signal Process.*, vol. 54, no. 2, pp. 613–626, 2006.
- [25] G. Mergen, V. Naware, and L. Tong, "Asymptotic detection performance of type-based multiple access over multiaccess fading channels," *IEEE Trans. Signal Process.*, vol. 55, no. 3, pp. 1081–1092, 2007.
- [26] A. Şahin, "Distributed learning over a wireless network with non-coherent majority vote computation," *IEEE Trans. Wireless Commun.*, vol. 22, no. 11, pp. 8020–8034, 2023.
- [27] —, "Over-the-air computation based on balanced number systems for federated edge learning," *IEEE Trans. Wireless Commun.*, Oct. 2023.
- [28] M. Goldenbaum and S. Stanczak, "Robust analog function computation via wireless multiple-access channels," *IEEE Trans. Commun.*, vol. 61, no. 9, pp. 3863–3877, 2013.
- [29] —, "On the channel estimation effort for analog computation over wireless multiple-access channels," *IEEE Wireless Commun. Lett.*, vol. 3, no. 3, pp. 261–264, 2014.
- [30] A. Kortke, M. Goldenbaum, and S. Stańczak, "Analog computation over the wireless channel: A proof of concept," in *Proc. IEEE Sensors*, 2014, pp. 1224–1227.
- [31] M. H. Adeli and A. Şahin, "Multi-cell non-coherent over-the-air computation for federated edge learning," in *Proc. IEEE International Conference on Communications (ICC)*, Apr. 2022, pp. 1–6.
- [32] J. Bernstein, Y.-X. Wang, K. Azizzadenesheli, and A. Anandkumar, "signSGD: Compressed optimisation for non-convex problems," in *Proc. International Conference on Machine Learning (ICML)*. PMLR, 2018, pp. 560–569.
- [33] A. Şahin and X. Wang, "Reliable majority vote computation with complementary sequences for UAV waypoint flight control," *IEEE Transactions on Wireless Communications*, pp. 1–14, 2024.
- [34] X. Chen, T. Chen, H. Sun, Z. S. Wu, and M. Hong, "Distributed training with heterogeneous data: bridging median- and mean-based algorithms," in *Proc. International Conference on Neural Information Processing Systems (NIPS)*. Red Hook, NY, USA: Curran Associates Inc., 2020.
- [35] Y. Miao, W. Ni, and H. Tian, "One-bit aggregation for over-the-air federated learning against Byzantine attacks," *IEEE Signal Processing Letters*, vol. 31, pp. 1024–1028, 2024.
- [36] J. H. Wilkinson, "The perfidious polynomial," *Studies in Numerical Analysis*, vol. 24, pp. 1–28, 1984.
- [37] D. Huffman, "The generation of impulse-equivalent pulse trains," *IRE Transactions on Information Theory*, vol. 8, no. 5, pp. 10–16, 1962.
- [38] P. Walk and W. Xiao, "Multi-user MOCZ for mobile machine type communications," in *Proc. IEEE Wireless Communications and Networking Conference (WCNC)*, 2021, pp. 1–6.
- [39] S. K. Dehkordi, P. Jung, P. Walk, D. Wieruch, K. Heuermann, and G. Caire, "Integrated sensing and communication with MOCZ waveform," 2023.
- [40] Y. Sun, Y. Zhang, G. Dou, Y. Lu, and Y. Song, "Noncoherent SIMO transmission via MOCZ for short packet-based machine-type com-

- munications in frequency-selective fading environments,” *IEEE Open Journal of the Communications Society*, vol. 4, pp. 1544–1550, 2023.
- [41] A. A. Siddiqui, E. Bedeer, H. H. Nguyen, and R. Barton, “Spectrally-efficient modulation on conjugate-reciprocal zeros (SE-MOCZ) for non-coherent short packet communications,” *IEEE Transactions on Wireless Communications*, vol. 23, no. 3, pp. 2226–2240, 2024.
- [42] E. Dahlman, S. Parkvall, and J. Skold, *5G NR: The Next Generation Wireless Access Technology*, 1st ed. USA: Academic Press, Inc., 2018.
- [43] B. Tegin and T. M. Duman, “Federated learning with over-the-air aggregation over time-varying channels,” *IEEE Trans. Wireless Commun.*, pp. 1–14, 2023.
- [44] M. H. Ackroyd, “The design of Huffman sequences,” *IEEE Transactions on Aerospace and Electronic Systems*, vol. AES-6, no. 6, pp. 790–796, 1970.
- [45] A. Şahin, R. Yang, E. Bala, M. C. Beluri, and R. L. Olesen, “Flexible DFT-S-OFDM: Solutions and challenges,” *IEEE Communications Magazine*, vol. 54, no. 11, pp. 106–112, 2016.
- [46] W. G. Horner and D. Gilbert, “A new method of solving numerical equations of all orders, by continuous approximation,” *Philosophical Transactions of the Royal Society of London*, vol. 109, pp. 308–335, 1819.
- [47] P. Langlois and N. Louvet, “How to ensure a faithful polynomial evaluation with the compensated Horner algorithm,” in *IEEE Symposium on Computer Arithmetic (ARITH)*, 2007, pp. 141–149.
- [48] L. A. Waller, B. W. Turnbull, and J. M. Hardin, “Obtaining distribution functions by numerical inversion of characteristic functions with applications,” *The American Statistician*, vol. 49, no. 4, pp. 346–350, 1995.
- [49] A. Şahin and R. Yang, “A generic complementary sequence construction and associated encoder/decoder design,” *IEEE Trans. Commun.*, pp. 1–15, 2021.
- [50] J. A. Davis and J. Jedwab, “Peak-to-mean power control in OFDM, Golay complementary sequences, and Reed-Muller codes,” *IEEE Trans. Inf. Theory*, vol. 45, no. 7, pp. 2397–2417, Nov. 1999.
- [51] M. Golay, “Complementary series,” *IRE Trans. Inf. Theory*, vol. 7, no. 2, pp. 82–87, Apr. 1961.